# *Tuning the self-assembly of the bioactive dipeptide L-carnosine by incorporation of a bulky aromatic substituent*

Article

Accepted Version

# Tuning the Self-Assembly of the Bioactive Dipeptide L-Carnosine by Incorporation of a Bulky Aromatic Substituent

**V. Castelletto,* G. Cheng, B. W. Greenland and I. W. Hamley,†**

*School of Chemistry, Food Science and Pharmacy, University of Reading, Whiteknights, Reading RG6 6AD, UK*

**P. J. F. Harris**

*Centre for Advanced Microscopy, The University of Reading, Reading RG6 6AF, UK*

* Author for Correspondence.

†Also at Diamond Light Source, Harwell Science and Innovation Campus, Chilton, Didcot, Oxfordshire OX11 0DE

**Abstract**

The dipeptide L-carnosine has a number of important biological properties. Here, we explore the effect of attachment of a bulky hydrophobic aromatic unit, Fmoc [*N*-(fluorenyl-9-methoxycarbonyl)] on the self-assembly of Fmoc-L-carnosine, i.e. Fmoc-β-alanine-histidine (Fmoc-βAH). It is shown that Fmoc-βAH forms well defined amyloid fibrils containing β-sheets above a critical aggregation concentration, which is determined from pyrene and ThT fluorescence experiments. Twisted fibrils were imaged by cryogenic transmission electron microscopy. The zinc-binding properties of Fmoc-βAH were investigated by FTIR and Raman spectroscopy since the formation of metal ion complexes with the histidine residue in carnosine is well known, and important to its biological roles. Observed changes in the spectra may reflect differences in the packing of the Fmoc-dipeptides due to electrostatic interactions. Cryo-TEM shows that this leads to changes in the fibril morphology. Hydrogelation is also induced by addition of an appropriate concentration of zinc ions. Our work shows that the Fmoc motif can be employed to drive the self-assembly of carnosine into amyloid fibrils.

## Introduction

The dipeptide L-carnosine (β-alanine-histidine, βAH) has a range of biological activities.[1-2] It has been shown to have antioxidant properties for carbohydrates (anti-glycation)[3-4] and lipids (anti-lipoxidation).[5] The presence of the β–alanine (βAH) residue is implicated in these roles, since it can react directly with oxidized carbohydrates and lipids.[6] The histidine (H) residue has properties including the ability to bind to transition metal ions. H-containing dipeptides such as L-carnosine (hereafter termed carnosine) are present in the mammalian brain within neuroglia and certain types of neurons.[7] Carnosine itself was first isolated from a meat extract and is present in muscle and nerve tissue, as well as the brain.[1-2] Its presence has been ascribed to its resistance to cleavage by intracellular proteases as well as the weak activity of specific carnosinases.[3] The important role of the H residue in carnosine is its ability to inhibit glycation-induced protein cross-linking.[7] This property may be important in the proposed application of carnosine to treat Alzheimer's disease.[7] It has also been shown to delay senescence of cultured cells,[8] which has been ascribed to the antioxidant properties of the peptide amongst other.[4] Carnosine also has a protective effect in inhibiting fibrillisation of α-crystallin during the formation of cataracts.[9-10] Derivatives of carnosine such as the methylated compound anserine (β-alanine-methylhistidine), homocarnosine (γ–aminobutyryl-carnosine) and others have also been isolated from tissue.[1, 11]

Despite its known bioactivity, there have been few studies on the physico-chemical properties of carnosine. Raman spectra of carnosine on silver nanoparticles (*via* Surface-Enhanced Raman Scattering) have been reported,[12] and a crystal structure has been published.[13]

Here, we explore the use of the Fmoc [Fmoc = *N*-(fluorenyl-9-methoxycarbonyl)] unit as a structure-directing agent to induce fibrillisation of

carnosine. Recent work has shown that bulky aromatic units such as Fmoc can be used to drive the self-assembly of short peptides *via* π-stacking interactions.[14-22] The Fmoc unit is a bulky aromatic substituent, used routinely as a protective group in solid phase peptide synthesis but generally cleaved from the N-terminus following synthesis. Retaining the Fmoc unit provides a convenient means to direct π–π stacking interactions and hence fibrillisation. Here, we first show that carnosine itself does not form β-sheet fibrils but forms a random coil structure in aqueous solution. We then investigate the self-assembly of Fmoc-carnosine, i.e. Fmoc-βAH using a variety of spectroscopic and microscopic techniques.

Finally, we examine the interaction of Fmoc-βAH with zinc ions due to the important role of metal ions in forming complexes with carnosine.[23-26] It has been suggested that zinc-carnosine chelates can be used natural antioxidants *in vivo* [27] for the treatment of gastric ulcers and inflammations. Since it is known that zinc ions form chelates with the imidazole ring in the H residue of carnosine,[23-24] it is expected that Fmoc-βAH can also induce zinc chelation. On that basis, we investigate in this work the self-assembled structure and chelation sites of Fmoc-βAH/$Zn^{2+}$ complexes, to obtain information about the properties of this new peptide derivative.

## Experimental

***Materials.*** The dipeptide βAH was purchased from Sigma-Aldrich (UK) and used as received. A portion of the Fmoc-βAH (Scheme 1) was synthesized in our laboratory by standard Fmoc solid-phase peptide synthesis techniques, while another portion was purchased from C S Bio Co (USA). In aqueous solution, the imidazole moiety is known to exist as an equilibrium of two tautomeric forms (I and II, Scheme 1).[23] The tautomers are distinguished by the position of one of the double bounds and the protonation level of the nitrogen atoms in the ring. Thus, both Nτ and $N_{\Pi}$ are

possible chelation sites for $Zn^{2+}$ ions, in addition to the numerous heteroatoms in the remainder of the Fmoc-βAH system.

***Synthesis and purification of Fmoc-βAH in our laboratory*** HOBt (1-hydroxybenzotriazole), HBTU [2-(1H-benzotriazol-1-yl)-1,1,3,3-tetramethyluronium hexafluorophosphate] and Fmoc- His(Trt) -Wang resin (100-200 mesh, 0.6 mM/g) were purchased from Novabiochem (UK). Anhydrous N,N-dimethylformamide (DMF) and trifluoroacetic acid (TFA) were purchased from Sigma-Aldrich (UK); acetonitrile (HPLC grade) and water (HPLC grade) were purchased from Fisher Scientific (UK).

Fmoc-βAH was synthesized on a 0.45 mM scale using a standard Fmoc chemistry procedure with a sintered glass funnel. After the resin was swollen in DMF for 30 min it was drained and treated with piperidine in DMF (1: 4 v/v) to deprotect the Fmoc group. The reaction mixture was agitated for 10 min by bubbling nitrogen through it, then drained. The piperidine treatment was repeated three times and then the resin was drained and washed with DMF (6 x). Later, the resin was allowed to react with activated Fmoc-βAH. Fmoc-βAH (3 eq. to resin loading) and 3 eq. HBTU / HOBt were dissolved in DMF (6 ml). Subsequently, 5.0 eq. $(^{i}Pr)_2NEt$ were added to the mixture, which was stirred for 5 minutes prior to being added to the drained resin. The coupling reaction of the activated Fmoc-βAH with the drained resin was agitated for 1.5 h by nitrogen bubbles, drained and washed with DMF (6 x), MeOH (4 x), and $CH_2Cl_2$ (4 x). In the cleavage step, the obtained Fmoc dipeptide attached to the solid support was treated with a mixture of 95% TFA, 2.5% triisopropylsilane, and 2.5% water. The mixture was stirred at room temperature for approximately 4 hrs, followed by filtration. The cleaved resin was washed three times with TFA. The obtained peptide solution was collected and concentrated by evaporating TFA under vacuum, followed by precipitation in cold diethyl ether. The crude product was separated by centrifugation and decanting the supernatant. The crude peptide was redissolved in

HPLC grade water with acetonitrile co-solvent and purified by reverse phase HPLC. Preparative reverse-phase HPLC was carried out on Perkin Elmer 200 system using a C18 column (Macherey-Nagel, 7μm, 10mm × 250mm) at 35°C (Perkin Elmer Series 200 Peltier Column Oven) with a UV/vis detector. The eluents, 0.1% TFA in acetonitrile and 0.1% aqueous TFA, were used as a gradient solvent system in the reverse-phase HPLC, where the acetonitrile portion increased linearly from 0% to 90% over 20 min and then decreased linearly to 0% over 10 min with a flow rate of 4 ml/min. The UV/vis detector monitored the sample elution at 254 nm. The fractions of the peptide were collected (retention time: 13 min) and after lyophilization, gave a white powder which was characterized by electrospray-mass spectroscopy (ES-MS) and $^{1}$H NMR. **Fmoc-βAH** : 1H NMR (400MHz, MeOH-$d_4$) δ (ppm): 8.78 (d, J = 1.2 Hz, 1H), 7.83 (d, J = 7.2 Hz, 2H),7.66 (d, J = 8.0 Hz, 2H), 7.41 (t, J = 7.6 Hz, 2H), 7.32 (m, 3H), 4.79 ( dd, $J_1$ = 8.4 Hz, $J_2$ = 5.2, 1H), 4.36 (d, J = 6.8 Hz, 2H), 4.22 (t, J = 6.8 Hz, 1H), 3.32 (m, 3H), 3.12 (dd, $J_1$ = 15.4 Hz, $J_2$ = 8.8, 1H), 2.44 (t, J = 6.8 Hz, 2H). MS: calc. $[M+1]^+$ = 449.17, found. $[M+1]^+$ = 449.18.

***Synthesis and purification of Fmoc-βAH by C S Bio***. Five grams (4 mM) of His-Cl-Trityl Rx (sub 0.8 mM/g, Lot 2054) in DMF was coupled with 3 eq. of Fmoc-βA using DIC/HOBt (3 eq./3 eq.). Coupling time: 3 hrs. After air flow drying, the resin was cleaved in a cocktail of TFA/$H_2O$/TIS (95/5/5). Cleavage time: 2 hrs. After removal of TFA reagents, water was added to the crude peptide and the mixture was lyophilized overnight. Crude peptide was loaded onto RPHPLC column (2 inch) in two batches with a flow rate of 25 ml/min in a TFA (0.1%) buffer system, gradient 20-50% buffer B in 50 min (buffer A, 0.1% TFA in water; buffer B, CAN). Final product (1.6 g) was collected and lyophilized with a purity of > 95%.

***Solution and gel formation.*** βAH was dissolved in Milli-Q water to the desired concentration and mixed by gentle stirring. Fmoc-βAH proved to be less soluble than βAH in water. Therefore, Fmoc-βAH solutions and gels were dissolved in Milli-Q

water by sonication in an ultrasonic bath at 35-40°C for 5-10 minutes. Upon cooling to room temperature, samples were allowed to stand for over three hours. Gelation was verified by tube inversion. Binding of $Zn^{2+}$ by Fmoc-βAH was studied by dissolving the peptide in $ZnCl_2$ solutions, following the same method described for Fmoc-βAH solutions and gels in water. Metal binding was studied for different molar ratios Mr= $\frac{[ZnCl_2]}{[Fmoc-\beta AH]}$ = 0.25, 0.5, 1 and 2 ([ ] = molar concentration). All the solutions and gels studied in this work had pH ~ 3.

***Pyrene (Pyr) Fluorescence Spectroscopy.*** Spectra were recorded on a Varian Cary Eclipse Fluorescence Spectrometer with samples in 5 mm disposable plastic cuvettes. Pyr fluorescence assays were made using a sample containing only Pyr ($2.0x10^{-6}$ wt %), and a set of samples containing (0.02-0.18) wt % Fmoc-βAH dissolved in $2.0x10^{-6}$ wt % Pyr. All spectra were measured from 366 to 460 nm, using $\lambda_{ex}$= 339 nm.

***Circular Dichorism (CD).*** Spectra were recorded using a Chirascan spectropolarimeter (Applied Photophysics, UK). CD was performed using Fmoc-βAH or βAH dissolved in water (0.06 wt %) and loaded into cover slip cuvettes (0.1 mm thick). Spectra are presented with absorbance $A < 2$ at any measured point with a 0.5 nm step, 1 nm bandwidth and 1 second collection time per step at 20 °C.

***Fourier Transform Infra-red (FTIR) spectroscopy.*** Spectra were measured on a Nicolet Nexus spectrometer with DTGS detector. FTIR data was measured for 1 wt % peptide solutions in $D_2O$, containing pure Fmoc-βAH, pure βAH or mixtures of Fmoc-βAH and $ZnCl_2$ (Mr= 0.25, 0.5, 1 and 2). Samples were sandwiched between two $CaF_2$ plate windows (spacer 0.0125 mm) Spectra were scanned 128 times over the range of 4000-900 $cm^{-1}$. Data was corrected by baseline subtraction.

***Raman Spectroscopy in Solution****.* Raman spectra were recorded on a Thermo scientific NXR FT-Raman Module, equipped with a NXR genie detector. Solutions of

1 wt % Fmoc-βAH solution in water, or 1 wt % peptide containing $ZnCl_2$ (Mr= 0.25, 0.5, 1 and 2), were put in cylindrical glass vials, with 5 mm diameter. The laser power was set at 1 W. A spectrum was collected from 400 $cm^{-1}$ to 4000 $cm^{-1}$ with 15 $cm^{-1}$ interval, taking 2000 averages. The obtained data was corrected by baseline subtraction.

***Thioflavin T Fluorescence (ThT) Spectroscopy.*** Spectra were recorded at 20 $^{o}$C using a Perkin Elementar Luminescence spectrometer LS50B. A solution containing $2x10^{-3}$ wt% ThT in water was prepared and used as a solvent for Fmoc-βAH or βAH solutions (0.01-0.2 wt%). The samples were put in 0.5 cm thick quartz cells, and their fluorescence was measured using $\lambda_{ex}$= 440 nm.

***Rheology.*** Rheological properties were determined using a controlled stress TA Instruments AR-2000 rheometer. The viscosity of the samples was measured performing controlled shear rate experiments with a cone-and-plate geometry (cone radius= 20 cm; cone angle= 1$^{o}$). Experiments were conducted on samples containing 0.004-1 wt % Fmoc-βAH.

***Cryogenic-Transmission Electron Microscopy (Cryo-TEM).*** Experiments were performed at Unilever Research, Colworth (Bedford, UK). Solutions of Fmoc-βAH in water (1 wt %), or solutions of Fmoc-βAH (1 wt %) containing $ZnCl_2$ (Mr= 0.25, 0.5, 1 and 2), were blotted and vitrified using a Gatan Cp3 cryoplunge system. The samples were prepared at a controlled temperature of 22 ℃ and at a relative humidity around 90%. A 3-µl drop of each solution was placed on a 400-mesh copper TEM grid (Agar) covered with a perforated carbon film (plasma treated). The drop was automatically blotted and the sample was plunged into liquid ethane (−183 ℃) to form a vitrified specimen, then transferred to liquid nitrogen (–196℃) for storage. The specimen was examined in a JEOL JEM-2100 electron microscope at 200 kV, at temperatures below −175 ℃. Images were recorded digitally on a Gatan UltraScan 1000 cooled

CCD camera using DigitalMicrograph (Gatan) in the low-dose imaging mode to minimize beam exposure and electron-beam radiation damage.

***Transmission Electron Microscopy (TEM).*** Imaging was performed using a Philips CM20 TEM microscope operated at 200 kV. Droplets of a 1 wt % Fmoc-βAH solution were placed on Cu grids coated with a carbon film (Agar Scientific, UK), stained with uranyl acetate (1 wt %) (Agar Scientific, UK) and dried.

***Congo Red assay.*** A drop of a 7 wt % Fmoc-βAH gel was placed onto a glass microscope slide, and partially stained using a freshly prepared and filtered 1 wt % Congo red solution in water. The partially stained gel was then placed under a cover slip and observed with the microscope through crossed polarizers, using an Olympus BX41 polarized microscope.

***X-ray Diffraction (XRD).*** X-ray diffraction was performed on a stalk prepared by suspending a drop of 1 wt % Fmoc-βAH between the ends of wax-coated capillaries, and allowing it to dry. The stalks were mounted (vertically) onto the four axis goniometer of a RAXIS IV++ x-ray diffractometer (Rigaku) equipped with a rotating anode generator. The XRD data was collected using a Saturn 992 CCD camera.

## Results and Discussion

### *Self assembly of Fmoc-βAH in water*

In the following we will describe the self-assembly of Fmoc-βAH in pure water. In order to highlight the secondary structure formation in Fmoc-βAH solutions, selected results obtained for Fmoc-βAH solutions will be compared with those obtained for βAH solutions.

Addition of the Fmoc unit leads to a substantial increase in hydrophobicity, as quantified for example by the octanol-water partition coefficient, which increases from log *P* = -3.7 for βAH to log *P* = 0.483 for Fmoc-βAH, as computed using web-based

software.[28] It is therefore possible the Fmoc-βAH in solution possesses a critical aggregation concentration (*cac*) resulting from hydrophobic interactions.

Pyr fluorescence studies were performed in order to determine the *cac* for Fmoc-βAH in water. This technique is routinely used to determine the critical micellar concentration for amphiphiles.[29-32] It is based in the analysis of the fluorescence intensity of the 0-0 band at $\lambda$ ~ 373 nm, denoted $I_1$, and the fluorescence intensity of the ratio $I_1/I_3$ ($I_3$: third principal vibronic band at $\lambda$~ 383 nm).[33] We have used Pyr fluorescence in the past to determine the *cac* for FFFF-PEG3k [34] and βAβAKLVFF-PEG3k,[35] while values of the *cac* for the β-amyloid peptide were also obtained by changes in the fluorescence of Pyr.[36]

The inset in Figure 1a shows representative examples of the fluorescence emission spectra measured for samples containing 0.02-0.18 wt % Fmoc-βAH and $2x10^{-6}$ wt % Pyr. The emission spectrum of Pyr ($\lambda_{ex}$= 339 nm) is characterized by the strong fluorescence of the 0-0 band ($\lambda$ ~ 373 nm), denoted as $I_1$ [33] (inset Figure 1a). Changes in $I_1$ reflect the variations of the lifetime of the excited state of Pyr, which is significantly different for different probe surroundings.[30] For amphiphilic solutions, a substantial increase in $I_1$ upon adding amphiphile to the solution, is due to the transfer of the amphiphile to a less polar domain (i.e. micellar core).[30] In this way, the *cac* can be pinpointed from the dependence of $I_1$ on the amphiphile concentration. The peak at 373 nm weakens significantly and merges into a shoulder on adding Pyr to a Fmoc-βAH solution. Nevertheless, it was possible to use the intensity at 373 nm to evaluate $I_1$, as a function of Fmoc-βAH concentration, for samples containing (0.02-0.18) wt % peptide in Figure 1a. For c> 0.07 wt % Fmoc-βAH, the Pyr absorbance at 373 nm increases substantially upon adding Fmoc-βAH to the solution, because the dipeptide is transferred to a less polar domain.[30] This phenomenon is correlated to the formation of aggregates (fibrils, as shown shortly)

and the insertion of the Pyr probe within the hydrophobic cores of the fibrils, for c> 0.07 wt % Fmoc-βAH.

The dependence of the ratio $I_1/I_3$ with the peptide concentration (Figure 1a) provides additional information about the self-assembly mechanism of Fmoc-βAH in water. The increase of $I_1/I_3$ with peptide concentration (Figure 1a) can be ascribed to a progressive decrease in the micropolarity of the environment containing the Pyr probe. This process can be understood as the formation of more compact peptide structures as the concentration of Fmoc-βAH is increased above the *cac*.

Similarly to the results shown in Figure 1a, it has been reported that the ratio $I_1/I_3$ increases upon addition of surfactant to solutions containing surfactant micelles.[37] This result was ascribed to the formation of more compact micelles with lower micropolarity, for micelles with higher surfactant content.

Figure 1b shows the solutions of the samples used to measure $I_1$ in Figure 1a. In good agreement with *cac* ~ 0.07 wt % Fmoc-βAH, the solutions become cloudy for c> 0.07 wt % Fmoc-βAH indicating the formation of large objects (i.e., long fibrils as shown shortly) that scatter light in the solution.

The secondary structure in solution was investigated by CD. Since this technique is only suitable for transparent solutions, only samples containing 0.06 wt % peptide were investigated. The obtained CD results, together with the corresponding absorbance spectra, are shown in Figure 2a and Figure 2b respectively. According to the results in Figure 1, the peptides in Figure 2 are not self assembled into long range ordered structures. Therefore, the CD spectra in Figure 2a may be expected to relate to the conformation of isolated molecules, not larger scale self assembled structures.

The CD spectrum for 0.06 wt % βAH is characterized by a strong positive band at ~ 214 nm (Figure 2a). This feature is associated to stacking interactions

(n→π* transition) of the imidazole ring, in analogy to similar results obtained for short peptides containing aromatic residues.[34, 38-42]

Stacking interactions of the aromatic units are still present for 0.06 wt % Fmoc-βAH, as it is denoted by the peak at 216 nm. Spectra with peaks in this region have been reported for Fmoc-tyrosine derivatives,[43-44] and Fmoc-peptides containing R, G and D residues.[45] However, the CD for 0.06 wt % Fmoc-βAH shows an additional peak at 222 nm (Figure 2a). This peak might indicate disruption in the packing of H residues for a population of molecules, since the CD spectra for random coil Poly-L-H (pH~3) is characterised by a maximum at 222 nm.[46-48]

The absorbance spectra corresponding to the CD data in Figure 2a shows no features for 0.06 wt % βAH. In contrast, the absorbance for 0.06 wt % Fmoc-βAH (Figure 2b) shows a maximum at 204 nm, which might arise from the imidazole ring,[49] and can be therefore associated to the disordered H residues.

It can be concluded from Figures 1 and 2 that it is necessary to study solutions with concentrations higher than 0.07 wt % to get an insight into the secondary structure of the self assembled objects. The secondary structure was then further studied by FTIR in the concentration regime c> 0.07 wt %.

The amide I band of the FTIR spectrum was analyzed for samples containing 1 wt % βAH or Fmoc-βAH, because it is sensitive to the secondary structure. The obtained results are displayed in Figure 3a with the significant peaks listed and identified in Table 1.

The FTIR spectrum for 1 wt % βAH (Figure 3a) is characterized by two strong bands[50] arising from the random coil or polyproline II-like conformation of βAH in solution (Table 1). In contrast, the FTIR spectrum for 1 wt % Fmoc-βAH (Figure 3a) suggests the presence of self assembled β-sheet structure (Table 1). The spectrum also shows a weak shoulder associated to TFA counterions (Table 1), since Fmoc-βAH was synthesized as a TFA salt. Finally, the peak at 1591 $cm^{-1}$ shows the

existence of $NH_4^+$ ions in the solutions (Table 1). $NH_4^+$ ions are present in the buffer during Fmoc-βAH purification and are still left in a small amount after lyophilisation, contributing to the peak at 1591 $cm^{-1}$ in the FTIR spectrum.

Additional information about the secondary structure of Fmoc-βAH was provided by Raman spectroscopy. Figure 3b shows that a 1 wt % solution of Fmoc-βAH presents several bands which can be easily identified (Table 2). The Raman spectrum shows the signature of a β-sheet structure,[51] and the imidazole ring in the H residue (Table 2).[23-24] Other peaks arise from the Fmoc unit,[52-53] or the C-O bond in the βA residue. Table 2 gives clear evidence of the tautomer II form (Scheme 1). In contrast, it is difficult to identify the contribution of the tautomer I, because the band at 1293 $cm^{-1}$ corresponds to both the Fmoc residue[52-53] and the imidazole ring in the form I[23-24] (Table 2).

Since FTIR and Raman results show the formation of β-sheet structures for higher concentrations of Fmoc-βAH, it is interesting to confirm whether this correlates to the formation of amyloid fibres. Therefore, binding of ThT to Fmoc-βAH was subsequently examined, since it is a dye staining method commonly used as a diagnostic for amyloid formation.[54-55] The fluorescence of the pure ThT sample, excited at $\lambda_{ex}$= 440 nm was characterized by a single broad peak centred at 482 nm (results not shown). The intensity of the fluorescence of the ThT peak was not affected by adding βAH to the ThT solution. In contrast, the intensity of the fluorescence at 482 nm showed a strong dependence on the Fmoc-βAH concentration.

Figure 4 shows the dependence of $I/I_o$ on βAH and Fmoc-βAH concentration. ($I$ = intensity of the ThT fluorescence peak for samples containing peptide, $I_o$ = the intensity of the fluorescence peak for a pure ThT solution). As expected, $I/I_o$ does not depend on the concentration for βAH since that peptide does not fibrillize in solution. It is evident from Figure 4 that for Fmoc-βAH enhanced ThT fluorescence is

observed, denoting the formation of peptide fibrils for concentrations greater than or equal than 0.04 wt % Fmoc-βAH. This result is in good agreement with the *cac* = 0.07 wt % Fmoc-βAH determined through Pyr assays in Figure 1.

It is clear from the Pyr fluorescence experiments that although the samples become slightly cloudy for c>0.07 wt%, the Pyr intensity increases with concentration. An analogous result was found for Tht fluorescence assays. It is evident from these results that the increase in fluorescence intensity arising from the binding of Pyr or ThT to fibrils overwhelms any effect associated with the formation of large objects (that scatter light) in the solution.

Results from the ThT fluorescence assays suggest that the number of fibrils in solution increases upon increasing the Fmoc-βAH concentration. This effect should also change the viscoelastic properties of the samples. The viscosity of the Fmoc-βAH samples was investigated by rheology. Figure 5 shows that the viscosity of the sample indeed increases steadily within the range (0.004-1) wt % Fmoc-βAH.

The self assembly of Fmoc-βAH was further studied by cryo-TEM. Figure 6a shows a cryo-TEM image obtained for a 1 wt % Fmoc-βAH sample. It contains individual fibrils, (15 ± 2) nm thick, some of them twisted around the main fibril axis.

The self assembly features of the sample in Figure 6a were also investigated in a dry film by TEM. Figure 6b shows a negative stain TEM image for a film dried from a 1 wt % Fmoc-βAH solution. Figure 6b shows long fibres, (6.9±0.8) nm thick. Although some fibrils in Figure 6b seem to be twisted, this cannot be unequivocally concluded from the TEM images. It has to be noted that the fibrils measured in the dried films (Figure 6b) are thinner than those measured in solution (Figure 6a), probably as a result of a dehydration effect.

TEM has been used in the literature as a tool to propose that Fmoc-dipeptides[56] and Fmoc-tripeptides[57] self assemble into nanotubes in aqueous solutions. In contrast, the structures revealed by TEM and cryo-TEM in Figure 6

correspond to twisted fibrils. According to the FT-IR data (Figure 3a, Table 1) the dipeptide motif in Fmoc-βAH is in an antiparallel β-sheet arrangement. Therefore, the fibril core might contain the βAH moiety while a fraction of the Fmoc units is exposed to the aqueous environment, during Fmoc-βAH self assembly. Although the Fmoc unit is highly hydrophobic, the exposure of this unit to water has already been suggested when modelling the structure of Fmoc-dipeptide[56] and Fmoc-tripeptide[57] nanotubes.

Further evidence for amyloid formation by Fmoc-βAH was provided by Congo red dye labeling experiments. Figure 7 shows the result for a 7 wt % Fmoc-βAH gel, partially stained with Congo red and observed through crossed polarizers. The sample shows regions of light grey birefringence, corresponding to the pure Fmoc-gel, coexisting with regions of blue birefringence caused by the Congo red staining (Figure 7). The presence of birefringence in the sample without the dye indicates that this peptide forms a liquid crystal phase for 7 wt % Fmoc-βAH.

X-ray diffraction from a dried stalk was also used to investigate the secondary structure of Fmoc-βAH. Figure 8 contains the 2D XRD pattern obtained for a stalk dried from a 1 wt % Fmoc-βAH solution. The inset in Figure 8 corresponds to the radial profile of the 2D XRD pattern. The pattern in Figure 8 presents a "cross β" pattern with reflections at 12.4 Å and 4.6 Å, indicating that the β-sheet structure is retained upon drying[58] and therefore indicates the secondary structure of the fibrils in Figure 6b.

Previous XRD patterns of Fmoc-$L_3$ peptide nanotubes displayed a sharp diffraction peak at 3.6 Å, associated to the π–π stacking between Fmoc residues.[57] The XRD pattern in Figure 8 contains a broad diffraction peak at 3.2 Å, which might be associated to the π–π stacking between Fmoc residues already deduced from the CD data in Figure 2a. The width of the peak at 3.2 Å indicates short range correlation of order (π–π stacking).

***Study of $Zn^{2+}$ binding by Fmoc-βAH in solution***

In the following we will study the formation of Fmoc-βAH/$Zn^{2+}$ complexes in solution. In particular, we will study $Zn^{2+}$ chelation by self-assembled Fmoc-βAH, above the *cac*.

$Zn^{2+}$ chelation by self-assembled Fmoc-βAH was studied for samples containing 1 wt % peptide with Mr= 0.25, 0.5, 1 and 2. Samples were first put into transparent glass tubes (Figure 9). Tube inversion and naked eye observation of the samples show that samples with Mr= 0.25 and 0.5 flow under tube inversion, but the sample with Mr= 1 is a gel which does not flow under tube inversion. The sample with Mr= 2 is cloudy and flows under tube inversion.

Cryo-TEM experiments were performed on samples shown in Figure 9, in order to examine the internal structure of the system. Figure 10 shows cryo-TEM photographs for 1 wt % Fmoc-βAH samples with Mr= 0.25, 0.5, 1 and 2. Samples with Mr= 0.25, 0.5 and 1 contain twisted fibrils (15±2) nm, (16±2) nm and (14±2) nm thick respectively (Figures 10 a-c). The sample with Mr= 2 contains twisted (14±2) nm thick fibrils, together with flexible and (48±22) nm thick nanotapes (Figures 10d-e).

The Debye screening length $D_L$ is the distance over which significant charge separation occurs. It can be shown that $D_L$= 1.3 μm for the sample with Mr= 2 (Figure 10 d-e), and it increases with decreasing [$ZnCl_2$] (Figures 10 a-c). So, $D_L$ does not seem to be related to fibril dimensions. The ionic strength of the solution would have to be much larger to give a nanoscale screening length. This raises the possibility that indeed $Zn^{2+}$ chelation takes place through binding to the imidazole ring of Fmoc-βAH. It has been reported in the literature that metal chelation by βAH can be pinpointed by specific wavelength shifts in FTIR and Raman spectra.[24] Therefore,

these spectroscopy techniques were used in the following to study the formation of Fmoc-βAH/$Zn^{2+}$ complexes.

The secondary structure of the samples was further studied by FTIR. The results obtained are shown in Figure 11a. Similarly to the FTIR results for the peptide in pure water (Figure 3a), the data for Mr= 0.25, 0.5, 1 and 2 samples (Figure 11a) is characterized by bands associated to the β-sheet and TFA and $NH_4^+$ ions (Table 1).

A weak shoulder at 1622 $cm^{-1}$ for the Mr= 0.25 sample, related to the tautomer II form,[24] smoothly turns into a well defined FT-IR band for the Mr= 2 sample (Figure 11a). Scheme 1 shows that metal coordination can affect the tautomeric equilibrium. Therefore, the progressive growth in tautomer II population (associated to the growth of the 1622 $cm^{-1}$ band in Figure 11a) is a consequence of $Zn^{2+}$ binding preferentially to $N_\tau$, resulting in a decrease in the tautomer I population.

Figure 11b shows the Raman spectra obtained for samples with Mr= 0.25-2 (1 wt% Fmoc-βAH). Raman spectra containing $ZnCl_2$ show similar features to those in Figure 3b, such that $Zn^{2+}$ chelation can be understood through changes in the Raman band positions, as a function of the $ZnCl_2$ content of the sample.

Unfortunately, due to the overlap of the band corresponding to the tautomer I form and the Fmoc moiety at 1293 $cm^{-1}$ (Figure 11b, Table 2), it is difficult to evaluate from the Raman results whether $Zn^{2+}$ chelation takes place through $N_\pi$ or $N_\tau$ binding. Nevertheless, it is evident from small shifts in the bands associated to the H ring (Figure 11b, Table 2), that the imidazole ring is involved in metal coordination. The dramatic decrease in intensity observed for the Raman bands at 1445 and 1293 $cm^{-1}$ for Mr= 2 (Figure 11b) also suggests the involvement of the imidazole ring in $Zn^{2+}$ chelation.

Chelation in the tautomer II configuration is revealed by the shifts in the band centred at 953 $cm^{-1}$ (Figure 11b, Table 2). In addition, a new band appears at 1614 $cm^{-1}$ for Mr= 2 (Figure 11b, Table 2), indicating chelation in the tautomer II form, in

comparison to the Raman spectra of metal-histidine complexes for which the $\nu C_4{=}C_5$ band at ~1600 $cm^{-1}$ indicates a $N_\tau$ binding to the metal ion.[59]

## Conclusions

In this work we studied the self assembly of Fmoc-βAH in aqueous media and the metal chelation of this peptide in $ZnCl_2$ solutions. We show that attachment of Fmoc leads to a fibrillar structure based on antiparallel β-sheets of bioactive carnosine moieties.

Pyr and ThT fluorescence experiments were used to determine a *cac* for Fmoc-βAH in water. Incorporation of the bulky aromatic Fmoc substituent leads to molecular amphiphilicity. In addition, aromatic π-stacking interactions contribute to drive self-assembly in fibrils. Cryo-TEM and TEM show that Fmoc-βAH forms twisted amyloid fibrils above the *cac*. FTIR and Raman spectroscopy confirmed that Fmoc-βAH fibrils contain β-sheets. The structure of the peptide fibrils in solution remains stable upon drying the aqueous sample, as confirmed by XRD and TEM results.

Fmoc-βAH/$Zn^{2+}$ chelation in $ZnCl_2$ solutions is studied for concentrations above the *cac*. Hydrogelation is induced by addition of an appropriate concentration of $Zn^{2+}$ ions. Cryo-TEM shows that addition of $ZnCl_2$ leads to a transition from twisted fibrils into wide nanotapes. Changes in the self-assembly motif might be controlled not only by electrostatic interactions, but also by $Zn^{2+}$ chelation. Indeed, the estimation of the Debye length suggests that $Zn^{2+}$ ions might be binding to Fmoc-βAH. This prediction is confirmed by FTIR and Raman data, which show sensitive changes in the spectra associated to $Zn^{2+}$ chelation.

Modifying βAH by incorporation of a terminal Fmoc unit may improve the efficiency of carnosine in applications in biotechnology, since Fmoc-βAH can form fibres while still chelating metal ions. In addition, hydrogelation can be induced (at sufficiently high concentration of $Zn^{2+}$ ions) presumably due to formation of a fibrillar

network. Hydrogelation may be a simple and useful detection or drug delivery system. Following these observations, incorporation of a terminal Fmoc unit in designed peptides might find other applications in diagnostic or delivery systems for healthcare.

**Acknowledgements** This work was supported by EPSRC grants EP/F048114/1 and EP/G026203/1. We are grateful to the Biocentre (University of Reading) for access to XRD facilities and Dr. R. Green for FTIR facilities. Use of the Chemical Analysis Facility and the Centre for Atomic Microscopy at the University of Reading is acknowledged. We acknowledge Steve Furzeland and Derek Atkins (Unilever, Colworth) for the cryo-TEM experiments.

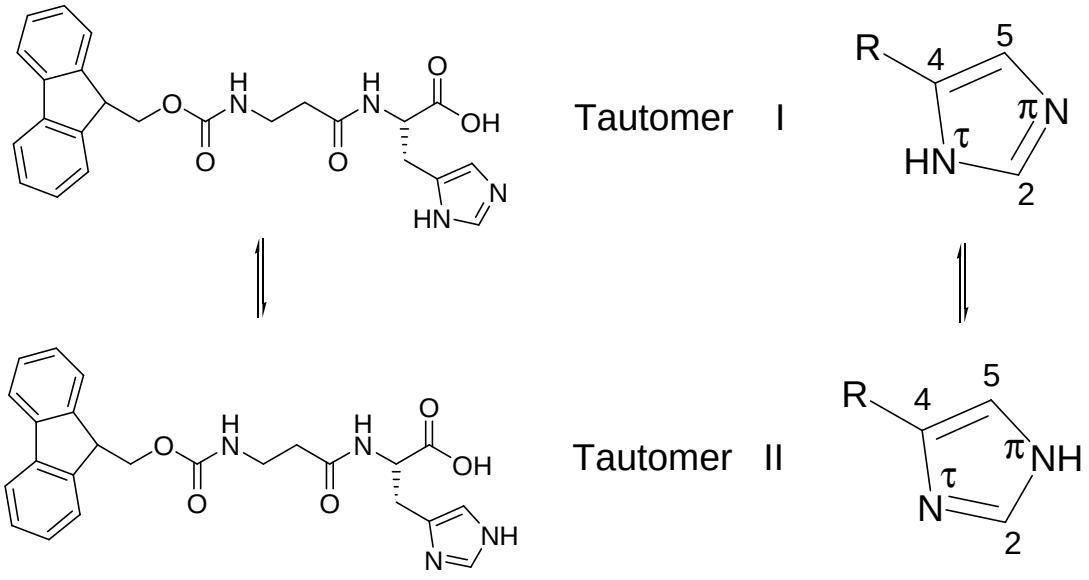


**Scheme 1** - Chemical structure of Fmoc-βAH together with the tautomer I and tautomer II configurations of the imidazole ring

**Table 1**: Wavenumbers ($cm^{-1}$) and assignments of the FTIR bands of βAH, and Fmoc-βAH.

| 1 wt% βAH | 1 wt% Fmoc-βAH | Assignments |
|---|---|---|
| 1638 $cm^{-1}$ | | amide carbonyl (C=O) absorption[60-61] |
| 1594 $cm^{-1}$ | | $NH_3^+$ group[60-61] |
| | 1684 $cm^{-1}$ | antiparallel β-sheet[51, 62-64] |
| | 1670 $cm^{-1}$ | TFA counterions[65-66] |
| | 1636 $cm^{-1}$ | antiparallel β-sheet[51, 62-64] |
| | 1591 $cm^{-1}$ | $NH_4^+$ ions |

**Table 2**: Wavenumbers ($cm^{-1}$) and assignments of main Raman bands of Fmoc-βAH and Fmoc-βAH/$Zn^{2+}$ complexes.

| Assignment | 1 wt% Fmoc-βAH | 1 wt% Fmoc-βAH Mr= 0.25 | 1 wt% Fmoc-βAH Mr= 0.5 | 1 wt% Fmoc-βAH Mr= 1 | 1 wt% Fmoc-βAH Mr= 2 |
|---|---|---|---|---|---|
| β-sheet[51] | 1627 | 1627 | 1627 | 1627 | 1661 |
| $\nu C_4=C_5$*[24] | ---- | ---- | ---- | ---- | 1614 |
| Fmoc[52] | 1475 | 1477 | 1477 | ---- | 1488 |
| δN-H*,$\delta CH_2$ [24] | 1445 | 1445 | 1445 | 1445 | 1435 |
| νC-N + ring breathing* [24] | 1343 | 1355 | ---- | 1343 | 1355 |
| Fmoc [52-53]+ tautomer I + ring breathing* [23] | 1293 | 1293 | 1293 | 1293 | 1293 |
| νNCN + δN-H* [24] | 1216 | 1233 | 1233 | 1226 | 1216 |
| C-O bond in the βA residue | 1127 | 1127 | 1127 | 1127 | ---- |
| δC-H*[24] | 1063 | ---- | 1063 | 1071 | 1083 |
| Fmoc[52] | 1024 | 1032 | 1031 | 1031 | 1031 |
| tautomer II+ δC-H* [23] | 953 | 953 | 953 | 944 | 987 |

Assignments: ν, stretching; δ, in-plane deformation; *, imidazole ring vibration

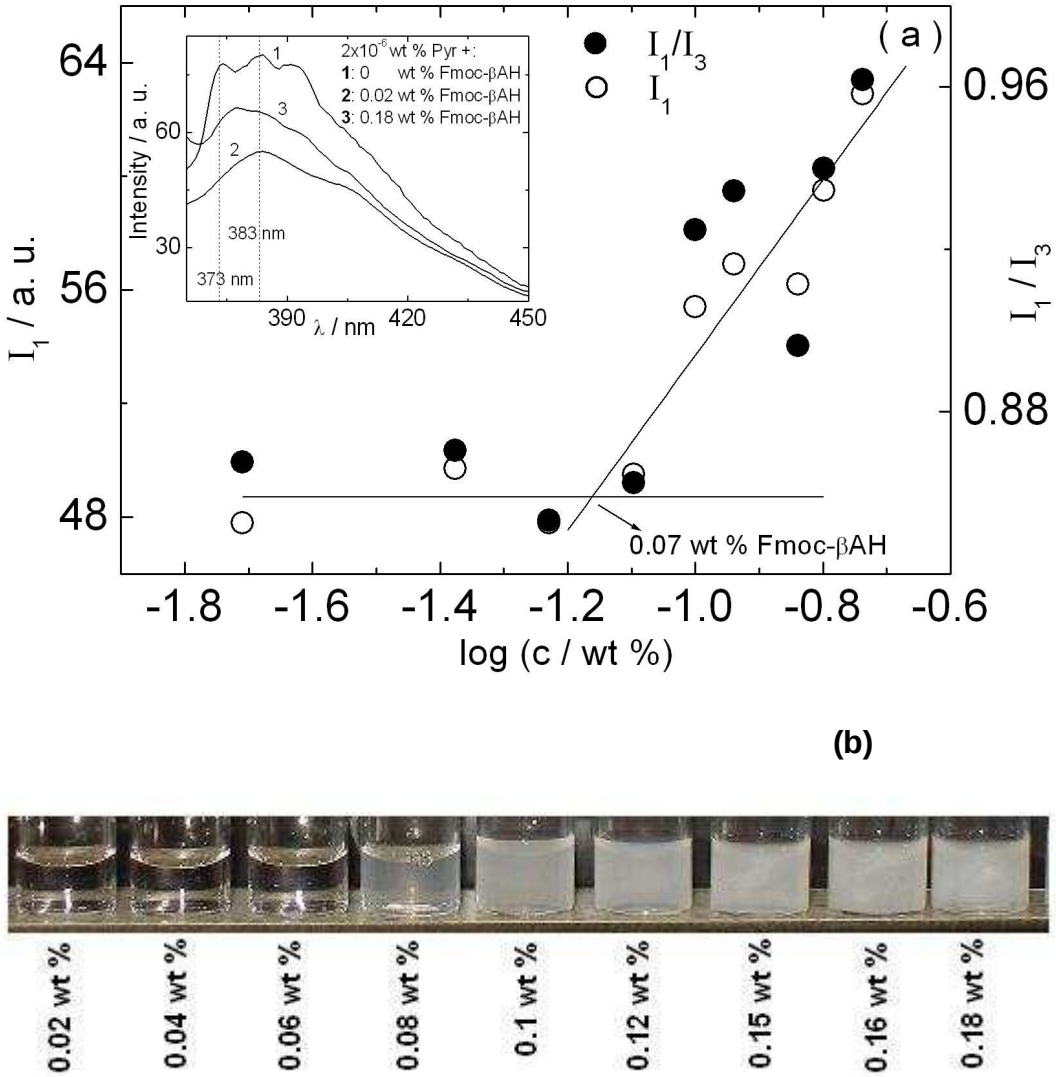


**Figure 1**. (a) Dependence of Pyr fluorescence intensities $I_1$ and $I_1/I_3$ as a function of the concentration. (b) Fmoc-βAH solutions used to measure the data in (a), containing 2x10$^{-6}$ wt % Pyr and 0.02-0.18 wt % Fmoc-βAH (as indicated in the figure)

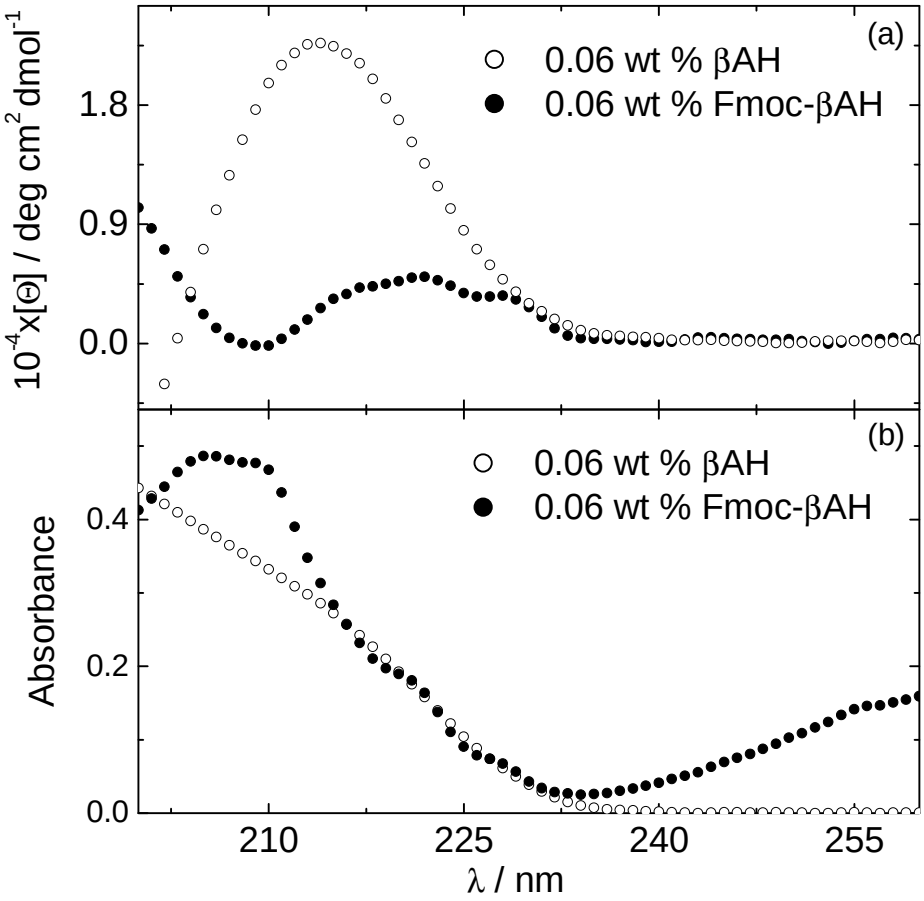


**Figure 2.** (a) CD and (b) absorbance data obtained for 0.06 wt % Fmoc-βAH and βAH.

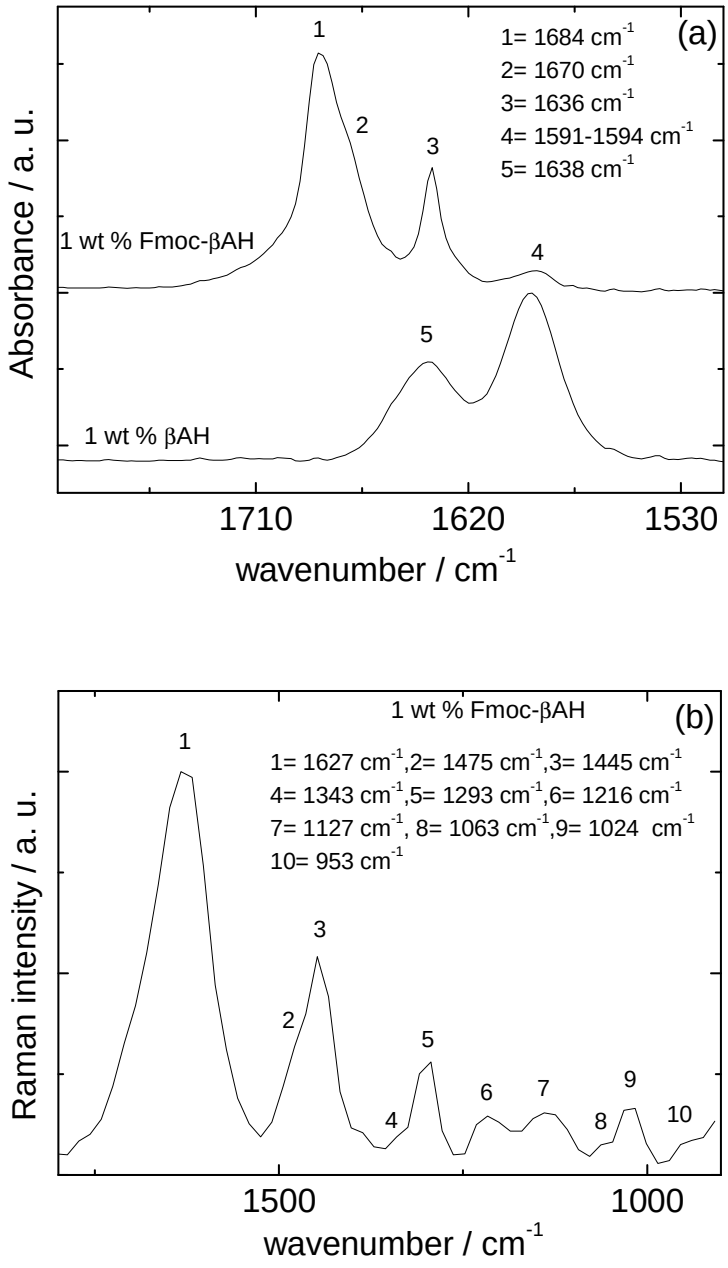


**Figure 3.** (a) FTIR data obtained for Fmoc-βAH and βAH solutions. The data has been shifted in order to enable visualization. (b) Raman data obtained for a Fmoc-βAH solution

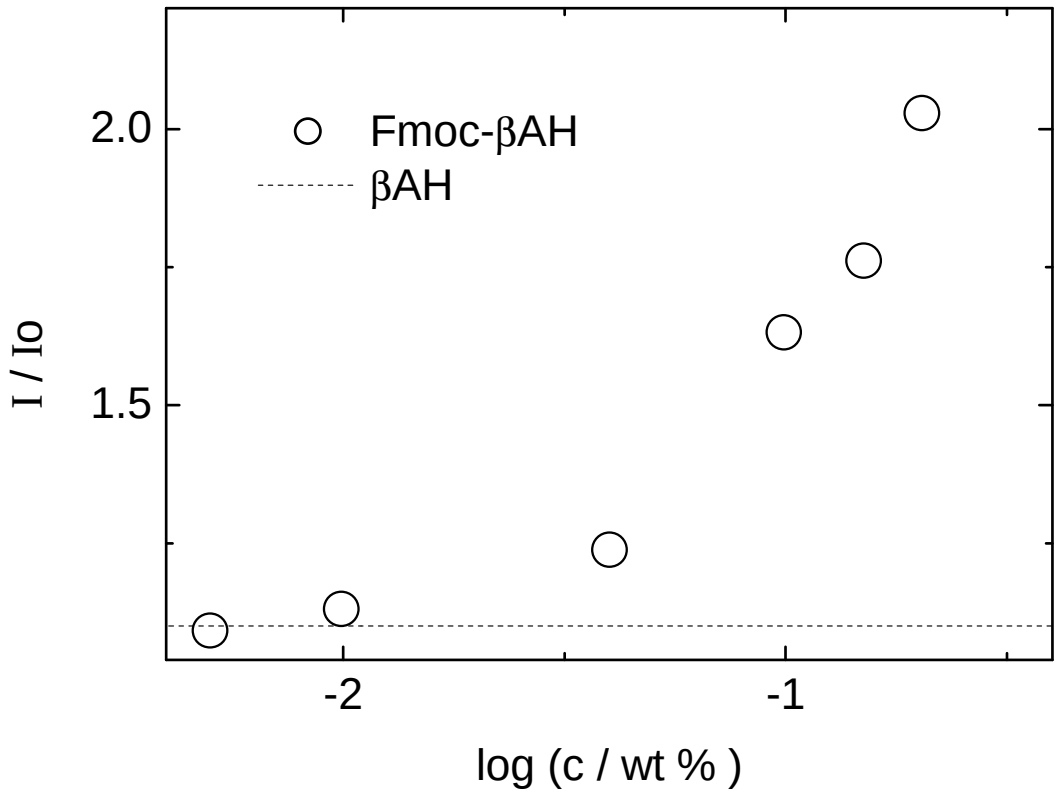


**Figure 4.** Intensity ratio of ThT fluorescence for samples containing Fmoc-βAH and βAH ($I$) normalized by the intensity of the pure ThT solution ($I_o$), plotted as a function of the peptide concentration

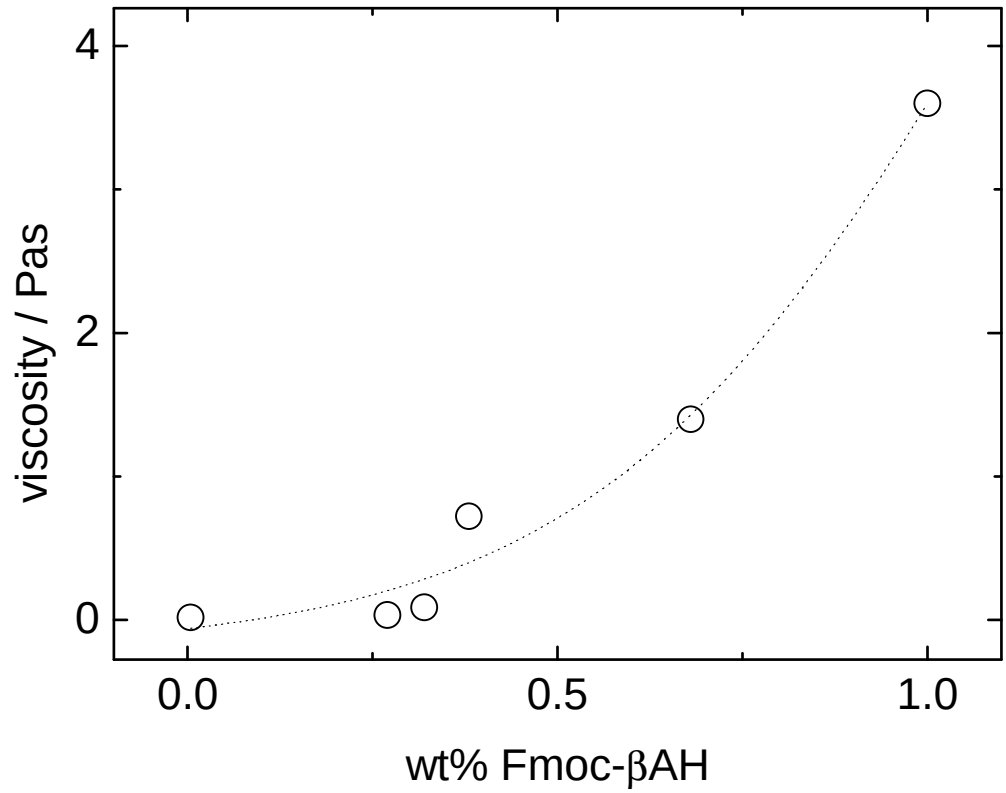


**Figure 5.** Viscosity at a shear rate= $9s^{-1}$ measured for Fmoc-βAH, as a function of the concentration

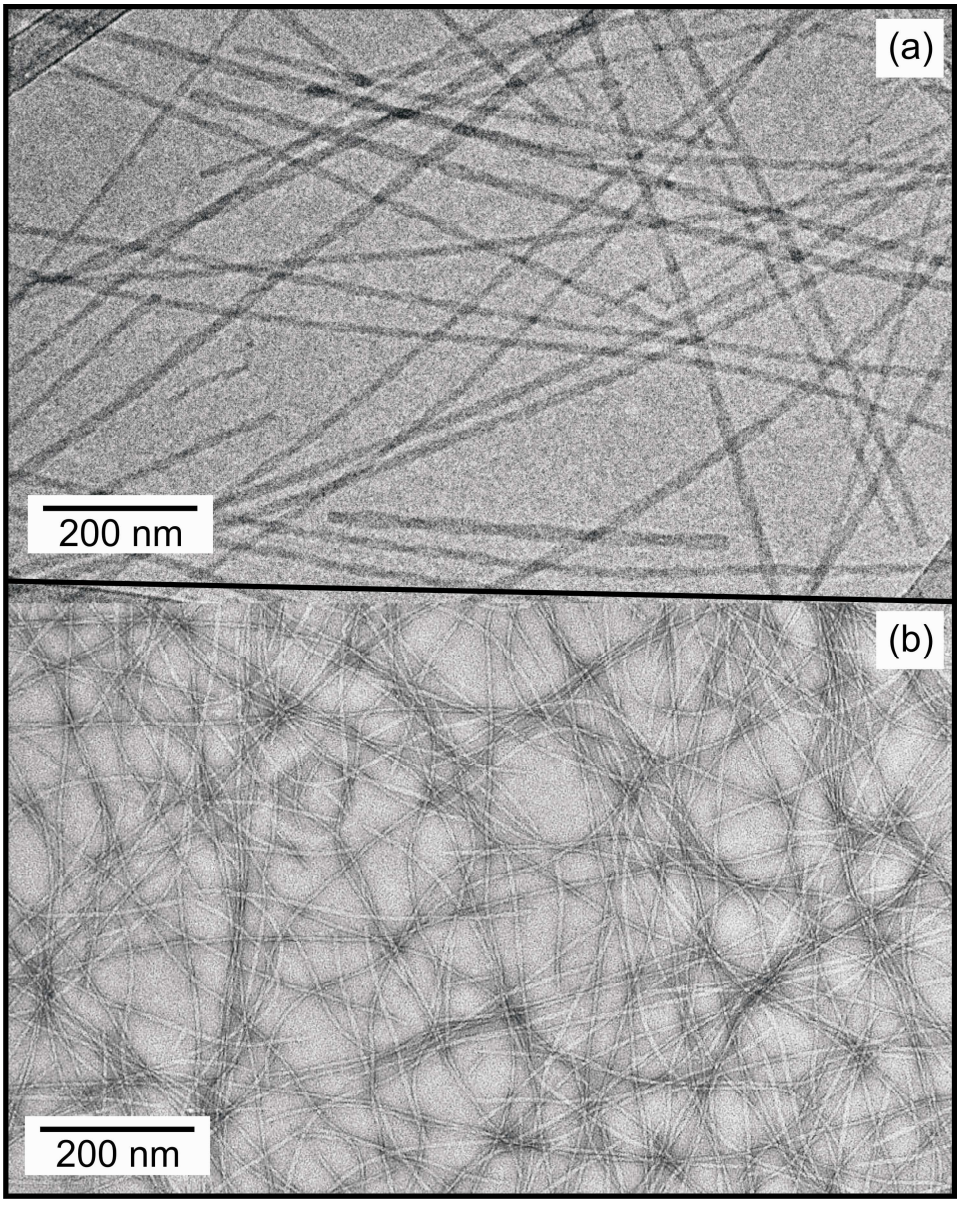


**Figure 6.** Images of 1 wt % Fmoc-βAH sample from (a) Cryo-TEM and (b) HR-TEM.

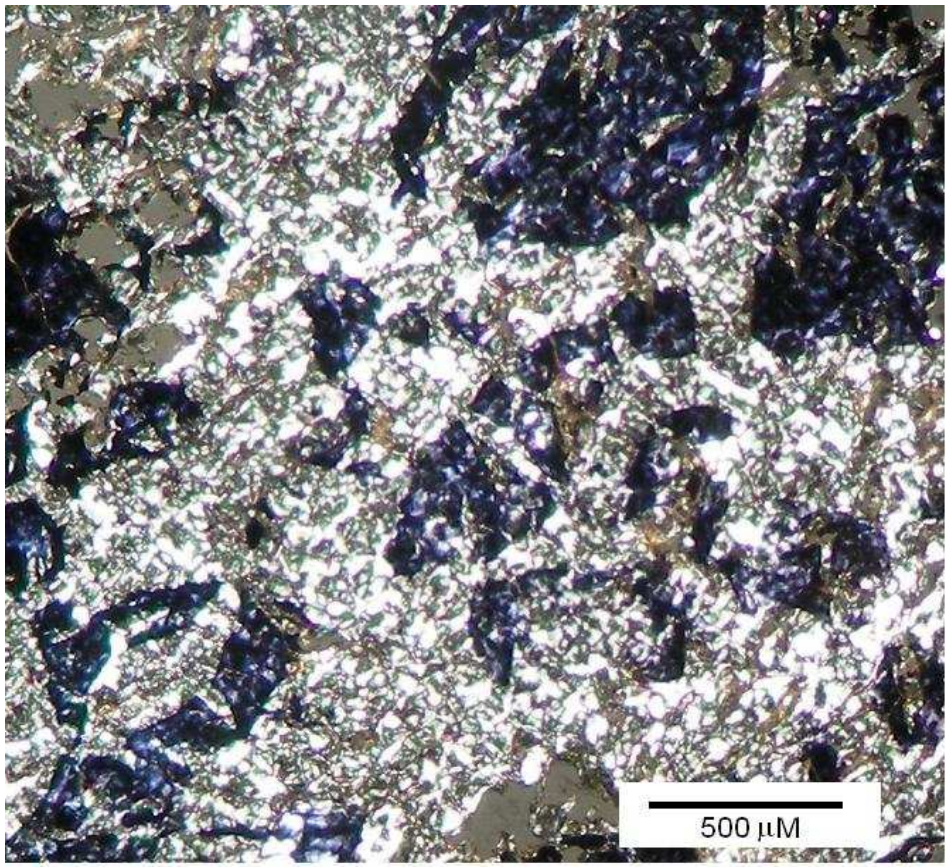


**Figure 7.** Optical micrograph of a sample stained with Congo red (7 wt % Fmoc-βAH).

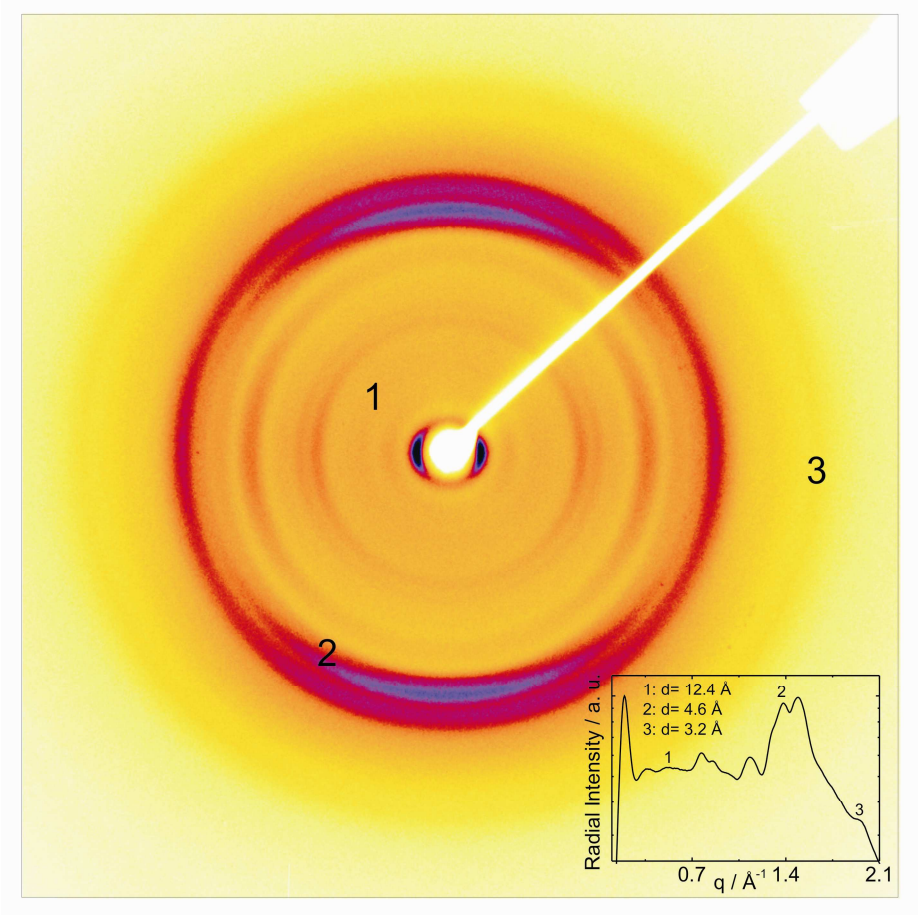


**Figure 8.** XRD 2D pattern obtained for a stalk dried from a 1 wt % Fmoc-βAH solution. The inset shows the radial average of the 2D-profile.

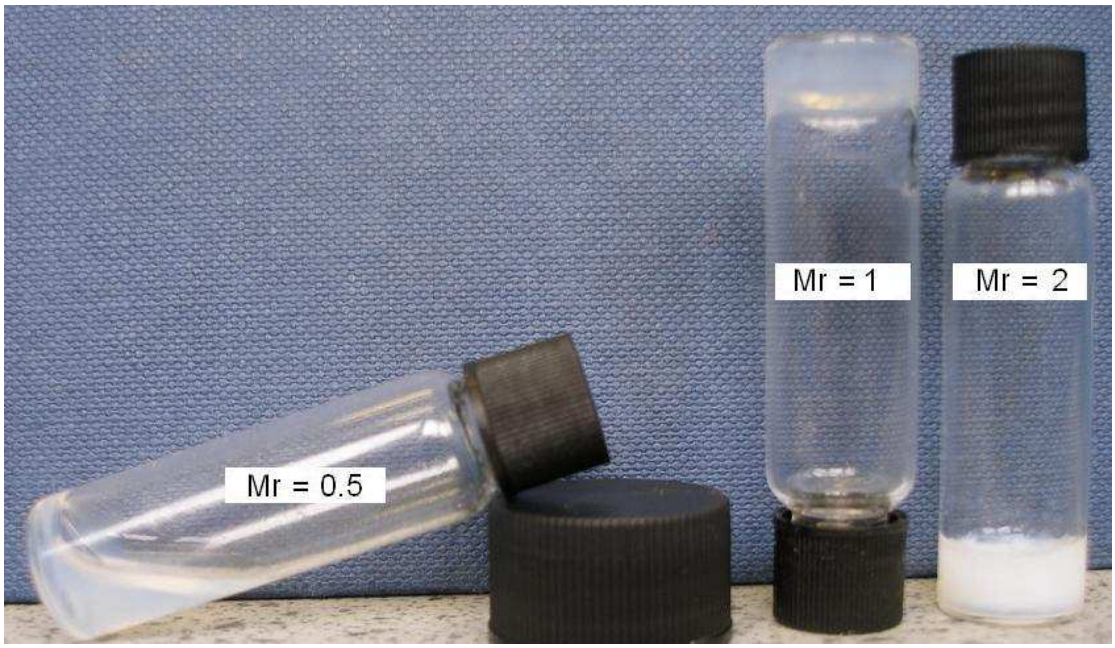


**Figure 9**. Glass vials containing 1 wt % Fmoc-βAH in $ZnCl_2$ solutions with Mr= 0.5, 1 and 2.

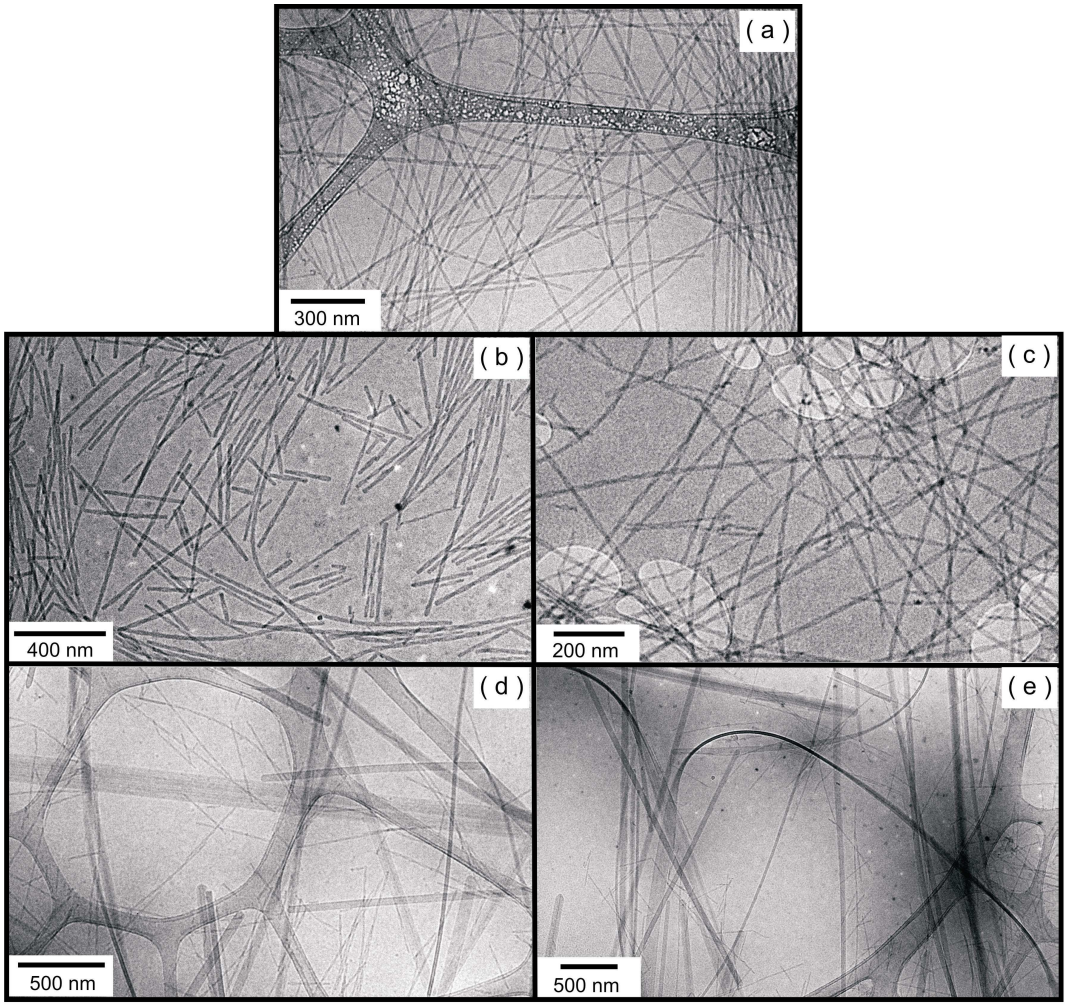


**Figure 10**. Cryo-TEM results for 1 wt % Fmoc-βAH in $ZnCl_2$ solutions with Mr= (a) 0.25, (b) 0.5, (c) 1 and (d-e) 2.

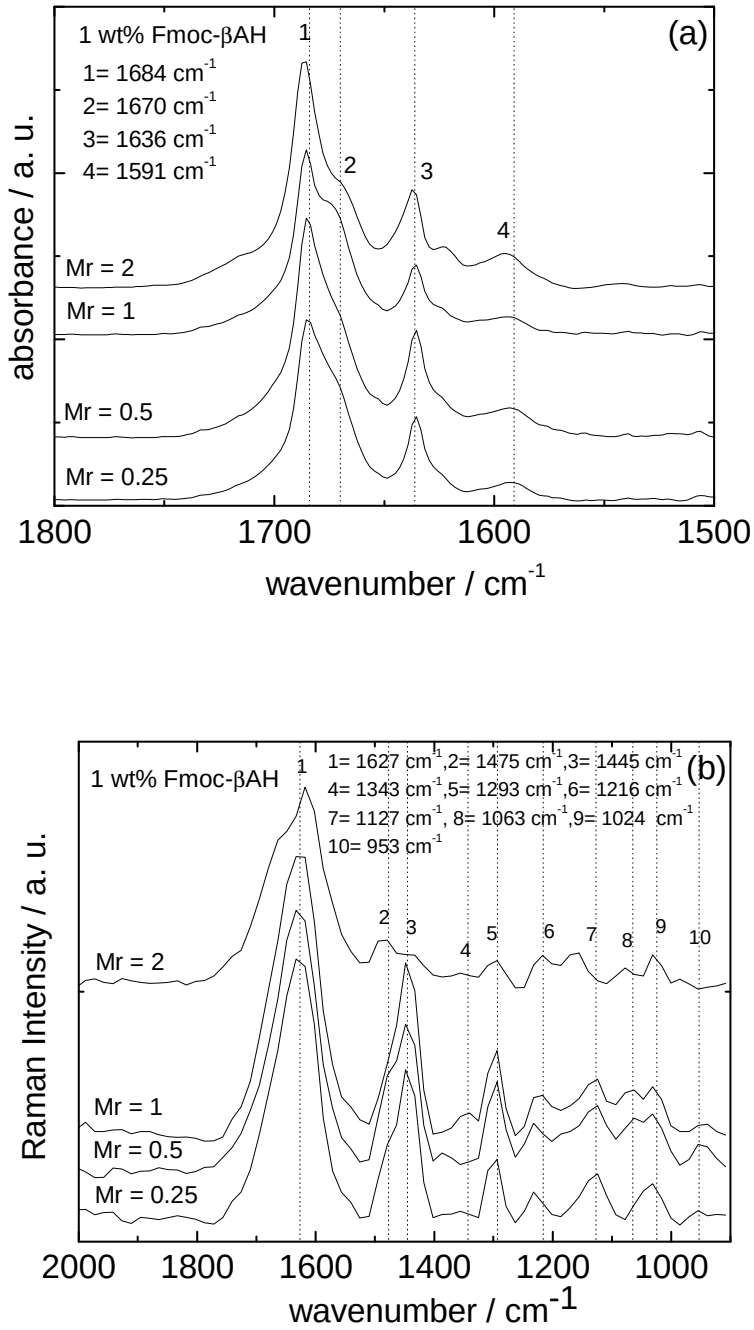


**Figure 11.** (a) FTIR and (b) Raman results for 1 wt % Fmoc-βAH solutions containing $ZnCl_2$ (Mr= 0.25, 0.5, 1 and 2). The data has been shifted in order to enable visualization. The broken lines indicate the position of the FTIR and Raman bands measured for 1 wt % Fmoc-βAH (Figure 3, Tables 1-2).

### *References*


(1) Gariballa, S. E.;Sinclair, A. J. *Age and Ageing* **2000**, *29*, 207-210.
(2) Bonfanti, L.;Peretto, P.;De Marchis, S.;Fasolo, A. *Prog. Neurobiol.* **1999**, *59*, 333-353.
(3) Hipkiss, A. R.;Michaelis, J.;Syrris, P. *FEBS Lett.* **1995**, *371*, 81-85.
(4) Brownson, C.;Hipkiss, A. R. *Free Radical Bio. Med.* **2000**, *28*, 1564-1570.
(5) Boldryev, A. A.;Dupin, A. M.;Bunin, A. Y.;Babizhaev, M. A.;Severin, S. E. *Biochem. Int.* **1987**, *15*, 1105-1113.
(6) Mehta, A. D.;Seidler, N. W. *J. Enzym. Inhib. Med. Chem.* **2005**, *20*, 199-203.
(7) Hobart, L. J.;Seibel, I.;Yeargans, G. S.;Seidler, N. W. *Life Sci.* **2004**, *75*, 1379-1389.
(8) McFarland, G. A.;Holliday, R. *Exp. Cell Res.* **1994**, *212*, 167-175.
(9) Seidler, N. W.;Yeargans, G. S.;Morgan, T. G. *Arch. Biochem. Biophys.* **2004**, *427*, 110-115.
(10) Attanasio, F.;Cataldo, S.;Fisichella, S.;Nicoletti, S.;Nicoletti, V. G.;Pignataro, B.;Savarino, A.;Rizzarelli, E. *Biochemistry* **2009**, *48*, 6522-6531.
(11) Brown, C. E.;Antholine, W. E. *J. Phys. Chem.* **1979**, *83*, 3314-3319
(12) Thomas, S.;Biswas, N.;Malkar, V. V.;Mukherjee, T.;Kapoor, S. *Chem. Phys. Lett.* **2010**, *491*.
(13) Barrans, Y.;Bellocq, A. M.;Cotrait, M.;Richard, H. *J. Mol. Struct.* **1976**, *30*, 225-242.
(14) Zhang, Y.;Gu, H.;Yang, Z.;Xu, B. *J. Am. Chem. Soc.* **2003**, *125*, 13680-13681.
(15) Toledano, S.;Williams, R. J.;Jayawarna, V.;Ulijn, R. V. *J. Am. Chem. Soc.* **2006**, *128*, 1070-1071.
(16) Jayawarna, V.;Ali, M.;Jowitt, T. A.;Miller, A. E.;Saiani, A.;Gough, J. E.;Ulijn, R. V. *Adv. Mat.* **2006**, *18*, 611-+
(17) Jayawarna, V.;Richardson, S. M.;Hirst, A. R.;Hodson, N. W.;Saiani, A.;Gough, J. E.;Ulijn, R. V. *Acta Biomat.* **2009**, *5*, 934-943
(18) Zhou, M.;Smith, A. M.;Das, A. K.;N.W., H.;Collins, R. F.;Ulijn, R. V.;Gough, J. E. *Biomaterials* **2009**, *30*, 2523-2530
(19) Mart, R. J.;Osborne, R. D.;Stevens, M. M.;Ulijn, R. V. *Soft Matter* **2006**, *2*, 822-835
(20) Mahler, A.;Reches, M.;Rechter, M.;Cohen, S.;Gazit, E. *Adv. Mat.* **2006**, *18*, 1365-+
(21) Adams, D. J.;Butler, M. F.;Frith, W. J.;Kirkland, M.;Mullen, L.;Sanderson, P. *Soft Matter* **2009**, *5*, 1856-1862.
(22) Cheng, G.;Castelletto, V.;Moulton, C. M.;Newby, G. E.;Hamley, I. W. *Langmuir* **2010**, *26*, 4990-4998.
(23) Torreggiani, A.;Fini, G.;Bottura, G. *J. Mol. Struct.***2001**, *565-566*, 341-346.
(24) Torregiani, A.;Bonora, S.;Fini, G. *Biopolymers* **2000**, *57*, 352-364.
(25) Lenz, G. R.;Martell, A. E. *Biochemistry* **1964**, *3*, 750-753.
(26) Lenz, G. R.;Martell, A. E. *Biochemistry* **1964**, *3*, 745-750.
(27) Tamba, M.;Torregiani, A. *Int. J. Radiat. Biol.* **1998**, *74*, 333.
(28) www.molinspiration.com. (2010).
(29) Johnsson, M.;Hansson, P.;Edwards, K. *J. Phys. Chem. B* **2001**, *105*, 8420-8430.
(30) Wilhelm, M.;Zhao, C.-L.;Wang, Y.;Xu, R.;Winnik, M. A.;Mura, J.-L.;Riess, G.;Croucher, M. D. *Macromolecules* **1991**, *24*, 1033-1040.

(31) Astafieva, I.;Zhong, X. F.;Eisenberg, A. *Macromolecules* **1993**, *26*, 7339-7352.
(32) Astafieva, I.;Khogaz, K.;Eisenberg, A. *Macromolecules* **1995**, *28*, 7127-7134.
(33) Johnsson, M.;Silvander, M.;Karlsson, G.;Edwards, K. *Langmuir* **1999**, *15*, 6314-6325.
(34) Castelletto, V.;Hamley , I. W. *Biophys. Chem.* **2009**, *141*, 169-174.
(35) Castelletto, V.;McKendrick, J. E.;Hamley, I. W.;Olsson, U.;Cenker, C. *Langmuir* **2010**, *26*, 11624-11627
(36) Sabaté , R.;Estelrich, J. *J. Phys. Chem. B* **2005**, *109*, 11027-11032.
(37) Abe, M.;Uchiyama, H.;Yamaguchi, T.;Suzuki, T.;Oginot, K. *Langmuir* **1992**, *8*, 2147-2151.
(38) Krysmann, M. J.;Castelletto, V.;Hamley, I. W. *Soft Matter* **2007**, *2*, 1401-1406.
(39) Krysmann, M. J.;Castelletto, V.;Kelarakis, A.;Hamley , I. W.;Hule, R. A.;Pochan, D. J. *Biochemistry* **2008**, *47*, 4597-4605.
(40) Castelletto, V.;Hamley , I. W.;Harris, P. J. F. *Biophys. Chem.* **2008**, *138*, 29-35.
(41) Castelletto, V.;Hamley, I. W.;Hule, R. A.;Pochan, D. J. *Angew. Chem. Int. Ed.* **2009**, *48*, 2317-2320.
(42) Hamley, I. W.;Krysmann, M. J.;Kelarakis, A.;Castelletto, V.;Noirez, L.;Hule, R. A.;Pochan, D. J. *Chem.- Eur. J.* **2008**, *14*, 11369-11375
(43) Yang, Z.;Xu, B. *Chem. Comm.* **2004**, 2424-2425
(44) Yang, Z.;Gu, H.;Fu, D.;Gao, P.;Lam, J. K. W.;Xu, B. *Adv. Mat.* **2004**, *16*, 1440.
(45) Cheng, G.;Castelletto, V.;Jones, R.;Connon, C. J.;Hamley, I. W. *Soft Matter* **2010**, in press.
(46) Peggion, E.;Cosani, A.;Terbojevich, M.;Scoffone, E. *Macromolecules* **1971**, *4*, 725-731.
(47) Beychock, S.;Pffumm, M. N.;Lehmann, J. E. *J. Am. Chem. Soc.* **1965**, *87*, 3990-3991.
(48) McCord, R. W.;Blakeney, E. W.;Mattice, W. L. *Biopolymers* **1977**, *16*, 1319-1329.
(49) Iwunze, M. O. *J. Photoch. Photobio.* **2007**, *186*, 283-289.
(50) Keiderling, T. A.;Xu, Q. (2002) Unfolded Proteins, (Rose, G. D., Ed.), pp 111-161, Academic Press Inc, San Diego.
(51) Haris, P.;Chapman, D. *Biopolymers* **1995**, *37*, 251-263.
(52) Due Lamen, B.;Christensen, D. H.;Holm, A.;Zher, R.;Faurskov Nielsen, O. *J. Am. Chem. Soc.* **1993**, *115*, 6247-6253.
(53) Ryttersgaarda, J.;Due Larsenb, B.;Holmb, A.;Christensena, D. H.;Faurskov Nielsena, O. *Spectrochim. Acta Part A* **1997**, *53*, 91-98.
(54) LeVine, H. *Protein Science* **1993**, *2*, 404-410.
(55) Nilsson, M. R. *Methods* **2004**, *34*, 151-160.
(56) Smith, A. M.;Williams, R. J.;Tang, C.;Coppo, P.;Collins, R. F.;Turner, M. L.;Saiani, A.;Ulijn, R. V. *Adv. Mat.* **2008**, *20*, 37-41.
(57) Xu, H.;Dasb, A. K.;Horiec, M.;Shaikae, M. S.;Smithae, A. M.;Luod, Y.;Lud, X.;Collinse, R.;Liemce, S. Y.;Songd, A.;Popelierce, P. L. A.;Turnerc, M. L.;Xiaoa, P.;Kinloch, I. A.;Ulijn, R. V. *Nanoscale* **2010**, *2*, 960-966.
(58) Morris, K.;Serpell, L. *Chem. Soc. Rev.* **2010**, *39*, 3445-3453.
(59) Miura, T.;Satoh, T.;Hori-i, A.;Takeuchi, H. *J. Raman Spectrosc.* **1998**, *29*, 41-47

(60) Lukton, A.;Sisti, A. *J. Org. Chem.* **1961**, *26*, 617-619.
(61) Baran, E. J.;Parajon-Costa, B. S.;Rojo, T.;Saez-Puche, R.;Fernandez, F.;Totaro, R. M.;Apella, M. C.;Etcheverry, S. B.;Torre, M. H. *J. Inorg. Biochem.* **1995**, *58*, 279-289.
(62) Stuart, B. (1997) *Biological Applications of Infrared Spectroscopy*, Wiley, Chichester.
(63) Rosler, A.;Klok, H.-A.;Hamley , I. W.;Castelletto, V.;Mykhaylyk, O. O. *Biomacromolecules* **2003**, *4*, 859-863.
(64) Miyazawa, T.;Blout, E. R. *J. Am. Chem. Soc.* **1961**, *83*, 712-719.
(65) Gaussier, H.;Morency, H.;Lavoie, M. C.;Subirade, M. *Appl. Environ. Microbiol.* **2002**, *68*, 4803-4808.
(66) Pelton, J. T.;McLean, L. R. *Anal. Biochem.* **2000**, *277*, 167-176.

Table of Contents image (TOC)

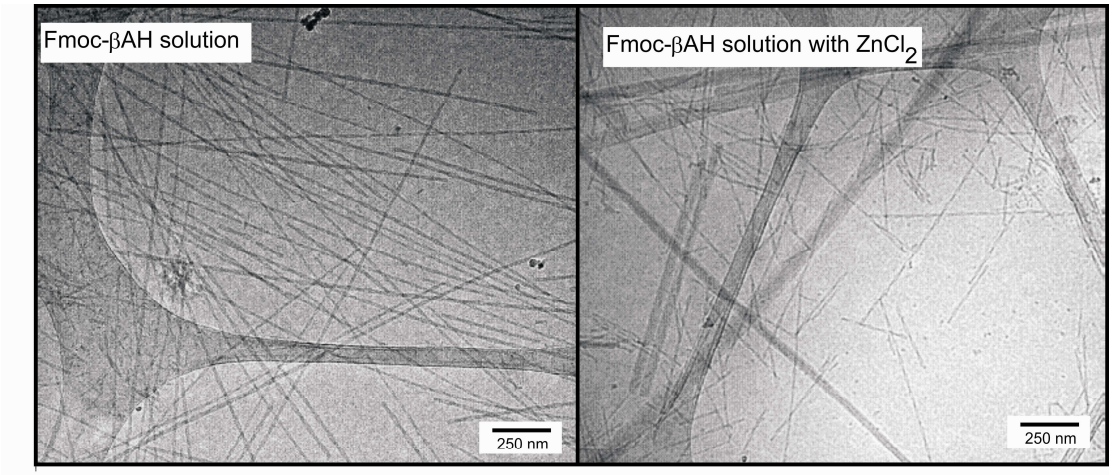


Addition of $ZnCl_2$ to solutions containing Fmoc-βAH fibres induces the co-existence of highly twisted fibres with wide flexible tapes.